

Nanoscale

Accepted Manuscript



This is an *Accepted Manuscript*, which has been through the Royal Society of Chemistry peer review process and has been accepted for publication.

Accepted Manuscripts are published online shortly after acceptance, before technical editing, formatting and proof reading. Using this free service, authors can make their results available to the community, in citable form, before we publish the edited article. We will replace this *Accepted Manuscript* with the edited and formatted *Advance Article* as soon as it is available.

You can find more information about *Accepted Manuscripts* in the [Information for Authors](#).

Please note that technical editing may introduce minor changes to the text and/or graphics, which may alter content. The journal's standard [Terms & Conditions](#) and the [Ethical guidelines](#) still apply. In no event shall the Royal Society of Chemistry be held responsible for any errors or omissions in this *Accepted Manuscript* or any consequences arising from the use of any information it contains.

ARTICLE

Hydrogel Pen for Electrochemical Reaction and Its Applications for 3D Printing

Cite this: DOI: 10.1039/x0xx00000x

Hosuk Kang,^{§a} Seongpil Hwang^{§*b} and Juhyoun Kwak^{*a}Received 00th January 2012,
Accepted 00th January 2012

DOI: 10.1039/x0xx00000x

www.rsc.org/

A hydrogel pen consisting of a microscopic pyramid containing electrolyte offers a localized electroactive area at the nanometer scale via controlled contact of the apex with a working electrode. The hydrogel pen merges the fine control of atomic force microscopy with non-linear diffusion of an ultramicroelectrode, producing a faradaic current that depends on the small electroactive area. The theoretical and experimental investigations of the mass transport behavior within the hydrogel reveal that the steady-state current from the faradaic reaction is linearly proportional to the deformed length of the hydrogel pen by contact, *i.e.*, signal transduction of deformation to an electrochemical signal, which enables the fine control of the electroactive area in the nanometer-scale regime. Combined with electrodeposition, localized electrochemistry of the hydrogel pen results in the ability to fabricate small sizes (110 nm in diameter), thick heights (up to 30 μm), and arbitrary structures, thereby indicating an additive process in 3 dimensions by localized electrodeposition.

Introduction

Three-dimensional (3D) printing is considered to be a key future technology for rapid prototyping and distributed manufacturing. In contrast to subtractive processes in conventional machining, 3D printing manufactures solid objects by an additive process that lays down successive layers of material. Although 3D printers based on various technologies have become commercially available, these technologies are limited with respect to feature size, cost, and range of materials, especially metals with high melting temperatures. Several efforts to achieve high resolution in 3D printing have led to the development of new approaches, including ink-based writing,¹ LIGA (lithography, electroplating, and molding),² holographic lithography,³ phase-mask lithography,⁴ and multi-photon fabrication,⁵ which all still have their own limitations. Despite increasing demand for 3D nanofabrication to investigate the unique properties of nanomaterials, the field of 3D printing at the nanometer scale is immature compared with well-developed 2D nanofabrication.⁶

Electrodeposition offers a low-cost, reliable, environmentally friendly, and versatile method to fabricate thin films of which the thickness is controlled between a monolayer and several micrometers.⁷ Although electrodeposition within templates⁸ and on the edge^{9, 10} provides a synthesis route for one-dimensional (1D) nanometer-scale metallic nanowires, electrodeposition for 3D geometries has hitherto only been partly explored. Nanoelectrodes¹¹ and nanopipettes¹²⁻¹⁵ combined with scanning electrochemical microscopy (SECM) have been the most common approaches, where metal ions generated at a nanoelectrode¹⁶ or delivered by nanopipettes are reduced to fabricate nanostructures on the surface of the electrode,¹⁷ so-called tip generation/surface collection (TG/SC) mode in SECM.¹⁸ Such innovative techniques, which have been

extensively developed by the Unwin group^{19, 20} and the Girault group,²¹⁻²³ make breakthrough for a localized electrochemistry. However, the developments of simple and high resolution SECM are still promising for fabrication and characterization of versatile nanomaterials.²⁴⁻²⁶

Here, we describe a novel hydrogel pen for electrochemistry and 3D printing based on electrodeposition by the hydrogel pen with a scanning probe system. Our hydrogel pen provides a unique alternative to nanopipettes for localized electrochemical reaction; it is also inexpensive and provides high resolution. The hydrogel pen is a microscopic hydrogel pyramid, of which the sharp apex is confined in a nanometer-scale region, and contains the electrolyte for electrochemical reaction. The contact between the tip of the hydrogel pen and a macroscopic electrode surface produces a nanometer-scale area for electrochemistry; we refer to this pen as a "hydrogel pen for electrochemical reaction" (HYPER). Despite a recent report of an electrical double layer at a hydrogel/electrode interface,²⁷ the literature contains sporadic reports on electrochemistry with a hydrogel electrolyte. In addition, the shape of the hydrogel near the working electrode also perturbs the mass transport behavior compared with that in a typical electrochemical reaction in solution. Therefore, the HYPER demands a detailed understanding of electrochemistry, including mass transport within the hydrogel pen near the electrode surface for various potential applications, including electrodeposition and imaging. The mass transport behavior in our hydrogel pen is investigated through simulation and experimental results for a redox probe to elucidate the relationship between the faradaic current and the deformation of an inert soft hydrogel. Additionally, on the basis of this novel electrochemical system, we address 3D printing by sequential and localized electrodeposition of platinum using the HYPER.

Results and discussion

Electrochemical behavior of Hydrogel Pen : Simulations and electrochemical measurements

The hydrogel pen in our experiments is a pyramid-shaped tip composed of agarose²⁸ and made from a master prepared by conventional photolithography and subsequent anisotropic etching (Figures 1A-C), similar to a previously reported polymer pen.²⁹ The hydrogel tip was filled with the electrolyte by being soaked in the electrolyte solution. When the sharp tip of a hydrogel pen is brought in contact with an electrode, a highly localized electrochemical reaction of redox species occurs on a small area of the electrode surface (Figure 1D). In contrast with nanopipettes and nanoelectrodes, in which the fabrication of glass itself is typically a daunting challenge, hydrogel pens provide simple methods for localized electrochemistry. In addition, the exact geometry of the hydrogel pen enables us to perform numerical simulations for better understanding of the electrochemical reactions in the hydrogel pen. Although agarose is poroviscoelastic owing to the combination of polymeric network deformation and water flow, plastic deformation of HYPHER is negligible in repeated approach-retraction experiments. (see supplementary information)

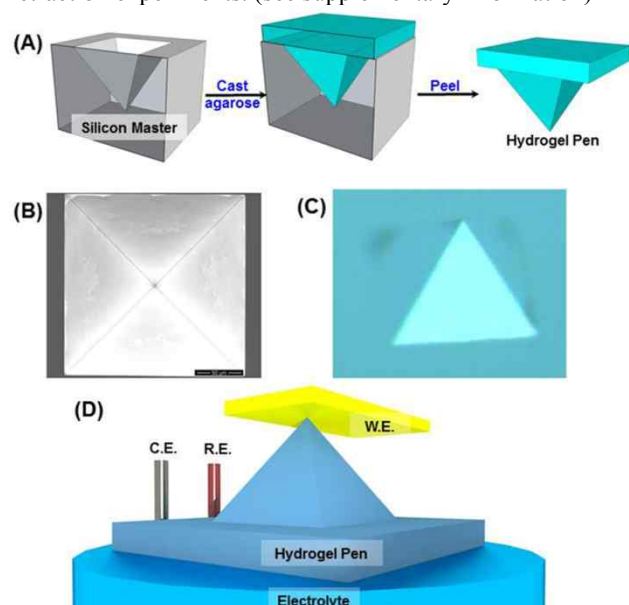


Figure 1. (A) A schematic illustration of the fabrication of the hydrogel pen. (B) Scanning electron microscopic image of the silicon master. Scale bar = 50 μm . (C) Optical microscopic image of the hydrogel pen. (D) Illustration of the electrochemical setup in which the hydrogel pen is used for localized electrochemistry.

The finite element method provides numerical simulations of electrochemistry within the HYPHER for cyclic voltammetry (CV) and chronoamperometry (CA). The contact area between the working electrode and the electrolyte was assumed to be flat and square as a consequence of the mechanical deformation of the hydrogel tip. Figure 2A shows the geometry for a simulation of the HYPHER in which the base length (B) and the height (H) of the pyramid are 200 μm and *ca.* 141 μm , respectively. When the HYPHER is pressed down d μm to the working electrode, an electroactive square with a side length of $\sqrt{2d}$ μm is formed. We hypothesized that no meniscus of the electrolyte is formed between the substrate and tip, that the

working electrode is not fouled, and that the original shape of the tip was not changed. In addition, we assumed that mass transport depends only on diffusion and that the charge transfer reaction is reversible; these assumptions are reasonable for the voltammetric oxidation of ferrocenemethanol at gold in a solution containing sufficient supporting electrolyte. Because the boundary of the pyramidal hydrogel tip is *ca.* 141 μm from the working electrode, the semi-infinite boundary condition is approximated, and the concentration at the boundary remains fixed. About the mass transport coefficient of ferrocenemethanol in agarose ($M_{\text{aga,FcMeOH}}$), $M_{\text{aga,FcMeOH}} = 0.94 \cdot M_{\text{sol,FCMeOH}}$, which has been determined experimentally using a diffusion-limited current with ultramicroelectrode contact with planar agarose³⁰ (Supplementary Information for simulation details and the determination of the mass transport coefficient in the gel). Previously, slower diffusion within agarose at interface than inside was reported indicating possible different local diffusion at surface.³¹ Diffusion within HYPHER in our experiments, however, is assumed to be homogeneous owing to high ionic strength and small hydrodynamic radius of solutes,³² although a detailed study on mass transportation within agarose is out of the scope of this paper. We also note that we used commercial finite element analysis software, even though the accuracy of the calculations might be diminished because of a lack of established theory related with HYPHER.³³

The simulated electrochemical behavior of HYPHER is very similar to that of typical ultramicroelectrodes. First, the cyclic voltammogram shows a well-known sigmoidal shape, indicating that the steady-state current is dominated by radial diffusion when $d = 1 \mu\text{m}$ (Figure 2B). Nonlinear diffusion within the HYPHER, however, is 52% of the radial diffusion of an in-laid-disk microelectrode with the same electroactive area in solution, as indicated by the steady-state currents that result from the pyramidal shape of the hydrogel pen (Figure 2B). Second, the cyclic voltammograms show a linear dependency of the steady-state currents on the compressed length of the tip (d), as shown in Figure 2C. Steady-state currents are linearly dependent not on d^2 (the electroactive square area) but on d , similar to typical behavior of ultramicroelectrodes. In addition, true steady-state currents are not observable on the voltammetric time scale when the tip deformation (d) is huge because of the decrease in the edge-to-area ratio. Notably, charging currents appear to be proportional to the contact area (d^2). Overall, the simulations indicate that the steady-state current is proportional to d , that the charging current is proportional to d^2 , and that these currents can be observed within a suitable experimental time scale.

Figure 2D shows simulated CA results for the HYPHER, demonstrating the Cottrell behavior in a short time regime and the steady-state current behavior in long time regime. Three questions arise concerning the CA of the HYPHER. First, is the current from the HYPHER truly steady state or does it decay gradually with time? Second, how much current is observed in the former case? Third, what is the effect of the meniscus between the tip and substrate? We inferred answers to these questions as follows: First, theory related to ultramicroelectrodes might offer insight into the behavior of the HYPHER despite the different shape of space for diffusion. Micropipettes have been shown to exhibit non-linear diffusion similar to that of in-laid disk ultramicroelectrodes but smaller because of the shape of the electrolyte.¹³ For this reason, currents from a square ultramicroelectrode are analogous to those from the HYPHER. A recent report from the Compton group demonstrates that a square ultramicroelectrode leads to

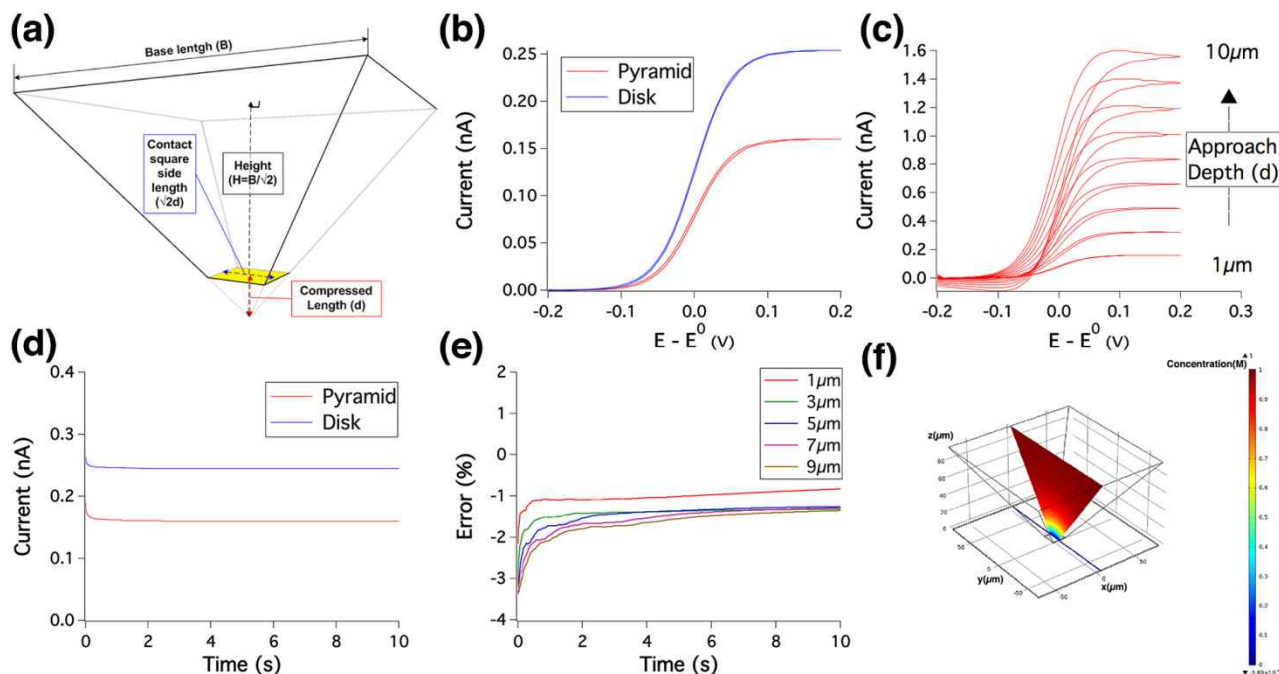


Figure 2. (a) Geometry for the simulation of the HYPER under the assumption of mechanical deformation of the tip. (b) Simulated cyclic voltammograms at a scan rate of 1 V/s for reversible charge transfer at the HYPER with $d = 1\ \mu\text{m}$ (red line) and at a disk ultramicroelectrode with the same electroactive area ($r = 0.798\ \mu\text{m}$, blue line). (c) Simulated cyclic voltammograms at the HYPER with various compressed lengths (1–10 μm) at a scan rate of 1 V/s. (d) Simulated chronoamperograms at the HYPER with $d = 1\ \mu\text{m}$ (red line) and at a disk ultramicroelectrode in the solution with the same electroactive area ($r = 0.798\ \mu\text{m}$, blue line) under a mass-transfer-controlled redox reaction. (e) Error vs. time plots for chronoamperograms with various compressed lengths calculated from equation (1) with respect to the numerical simulation. (f) Simulated steady-state diffusion-limited concentration profile of the HYPER with a meniscus.

the formation of a true steady-state current due to enhanced diffusion at the side and vertex,³⁴ whereas currents decay gradually with time in microband ultramicroelectrodes.³⁵ Therefore, the current from the HYPER in CA experiments is steady state or at least pseudo-steady state on the experimental time scale, although not to the extent of current from a square ultramicroelectrode. Second, the steady-state currents of HYPER are proportional to the side length, not to the square area, which is similar to the typical relationships observed in the case of ultramicroelectrodes.

A comparison of the chronoamperograms for the HYPER with those for an in-laid disk ultramicroelectrode of equal area in the electrolyte reveals that the steady-state current of the HYPER is *ca.* 52% of that of the ultramicroelectrode (Figure 2D). At short CA times, the Cottrell current dominates because of the thinness of the diffusion layer compared with the side length of the electroactive area. Therefore, the current of the HYPER in CA at the invasion length of d is semi-empirically determined as follows:

$$I \approx \frac{nFDC^*(\sqrt{2}d)^2}{\sqrt{\pi t}} + 0.520 \times (4nFDC^*\sqrt{\frac{2}{\pi}}d) \quad (1)$$

$$I_{ss} \approx 1.66nFDC^*d \quad (2)$$

where D is the diffusion coefficient within the hydrogel, F is the Faraday's constant, n is the number of electrons involved in the redox reaction, C^* is the bulk concentration of the redox species, and d is the compressed length of the HYPER. Figure 2E shows a comparison of equation (1) to a numerical simulation of the HYPER. Although the current behavior in the short time regime at large d shows a relatively large deviation, equation (1) describes the currents of the HYPER well at small d values (less than $3\ \mu\text{m}$) over the entire time regime. These results indicate that equation (1) and equation (2) are valid

approximations when the HYPER is operated with small d for typical scanning probe microscope (SPM) applications. The validity of these approximations is a very significant and attractive feature of the HYPER because the deformation of the hydrogel tip induces changes in the length of the square side, followed by changes in the steady-state current; *i.e.*, the electrochemical steady-state current provides the signal transduction to detect the mechanical deformation of an inert hydrogel tip. This electrochemical current could provide the feedback signal for SPM to control the electroactive area between the substrate and tip. In contrast, polymeric pens composed of Polydimethylsiloxane (PDMS) do not generate a signal that depends on the deformation of PDMS.^{29, 36} Therefore, electrochemistry within the HYPER might be a very useful technique for SPM requiring feedback signal to maintain constant tip-substrate interaction. Third, a water meniscus between the hydrogel pen and the working electrode might be inevitable,^{13, 37} which represents another electrolyte for electrochemistry. To avoid difficulties related to the shape of the meniscus depending on various factors such as the hydrophilicity of the substrate, we performed numerical simulations of the HYPER and a water meniscus under the assumption that the water meniscus is a simple hexahedron. The results indicate that the effect of a meniscus on the currents in the HYPER are negligible because the redox species in the thin layer is completely and quickly consumed and because the sluggish mass transport through the small contact area between the tip and meniscus hinders the supply of redox species. In Figure 2F, the concentration profile within the HYPER for a diffusion-limited redox reaction demonstrates the complete consumption of redox species in the meniscus and a higher mass transport at the edge in the HYPER. Overall, chronoamperograms of HYPER at small d is predicted to

generate a steady-state current linearly proportional to the compressed height (d) by the effects of the edge and vertex of the HYPER at a highly localized electroactive square, independent of the water meniscus.

The approach curve of the HYPER for the rapid oxidation of ferrocenemethanol under diffusion-limited conditions, in which the tip was sequentially lowered by $1\mu\text{m}$ every 10sec (Figure 3A), is in good agreement with the CA simulation results (Figure 3B). Before contact, no current was generated. When the HYPER contacts the working electrode for the first time, a sharp increase in current, which consists of both the charging current and the anodic current by the oxidation of ferrocenemethanol was observed. The charging current quickly disappeared because of small RC values; then, only a faradaic current was observed. When we increased the length of the square side by pressing the tip to the substrate, a linear increase in the steady-state current was observed, as predicted by the numerical simulation and equation (2) (blue line in Figure 3B). Notably, charging currents were also observed due to the increased contact area when the tip was pressed to the substrate. In addition, the steady-state currents deviated from equation (2) at larger d values, most likely because a smaller ratio between the perimeter and surface areas resulted in smaller edge diffusion. These experimental results demonstrate that the steady-state current is generated and is linearly proportional to the length of the square side of the deformed-pyramid-shaped hydrogel pen. Therefore, the area for electrochemistry is controlled by measuring this steady-state current. The cyclic voltammogram of the HYPER also shows the predicted sigmoidal shape depending on the size of contact area (Figure 3C). When d was greater than $5\mu\text{m}$, sigmoidal shaped voltammograms changed to the typical diffusion-controlled voltammograms, indicating that a contribution of edge diffusion to the overall mass transport of reagent is minor. When a constant-height SECM image was obtained on a well-defined gold compact discs (CDs), the variations in faradaic current directly represent the topography of CDs owing to change in d depending on the depth of disk groove. (See supplementary information. Figure S7) Overall, the HYPER provides a unique method to convert the mechanical deformation of an inert polymer into an electrochemical current signal and to localize the electrochemistry at the nanometer scale through control of the faradaic current without any special apparatus and to enhance current SECM technique for high-resolution imaging.

3-Dimensional Electrodeposition of Platinum using Hydrogel Pen

Electrodeposition within the small area defined by the HYPER was investigated to fabricate 3D metallic nanostructures. Platinum (Pt) film on Au was deposited electrochemically because Pt has unique properties in a wide range of heterogeneous catalytic applications.³⁸ First, the HYPER tip was brought into progressively closer proximity to the working electrodes at the potential of a no faradaic reaction until a charging current was observed by the contact between tip and working electrode. Pt was deposited by applying potential pulses,³⁹ the Pt was reduced quickly, and the consumed Pt cations in the diffusion layer were replenished for a relatively long time at higher potentials. Figure 4A shows SEM images of the electrodeposited tack-like Pt structure on Au. The thin layer of electrolyte meniscus might produce the round head of a tack.

After the Pt cations in the meniscus were reduced, the real

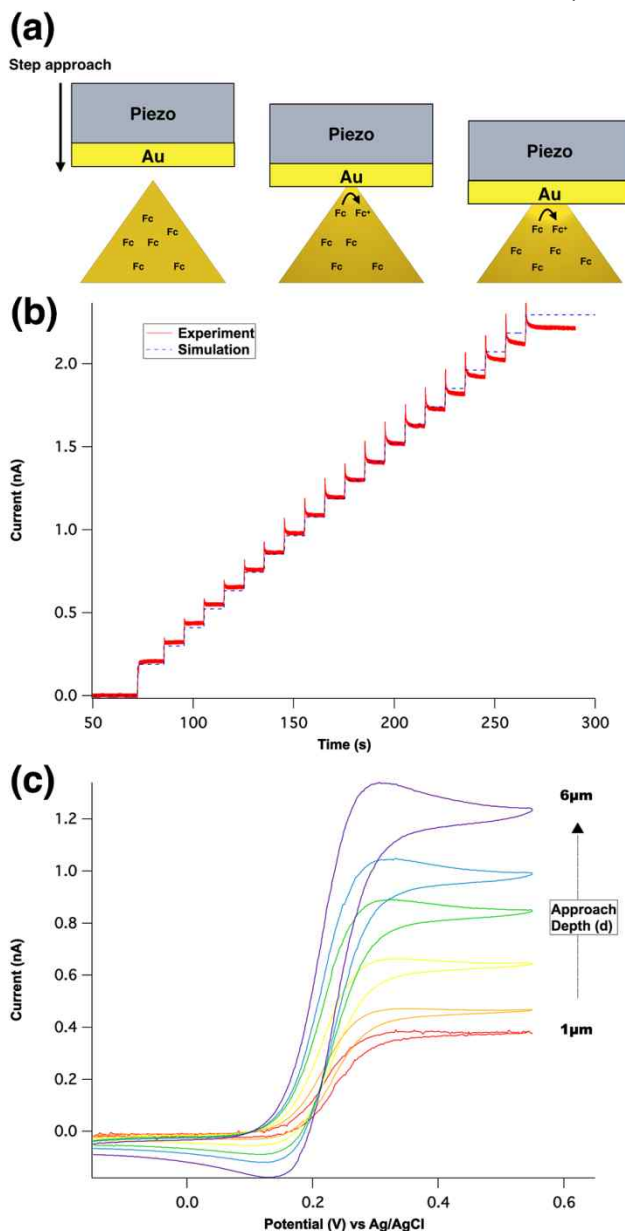


Figure 3. (a) Schematic diagram of the HYPER approach involving sequential pressing down of the electrode. (b) Current vs. time plot measured as the tip approached the working electrode ($1\mu\text{m}$ per every 10sec) at $E = 0.5\text{V}$ vs. Ag/AgCl . The dashed blue line represents theoretical currents calculated from equation (2). (c) Cyclic voltammograms of the HYPER at $d = 1\mu\text{m} - 6\mu\text{m}$ within the hydrogel containing 1mM FCMeOH and 0.115M KClO_4 . Scan rate = $50\text{mV}/\text{s}$.

contact area would be the only channel for supplying Pt cations through diffusion in the HYPER (*vide supra*), in which resulted in the formation of the pin of a tack, as shown in Figure 4B. The diameter and height of the Pt pin deposited by the HYPER are approximately 110nm and 270nm , respectively. When the side of the electroactive square by contact was increased to ca. $20\mu\text{m}$, electrodeposition yielded square Pt, as expected, in which the electroactive area of the HYPER was much larger than the surrounding meniscus (Figure 2C). By adjusting the time for pulse deposition, we deposited a thicker Pt structure of ca. $1.7\mu\text{m}$. Notably, electrodeposition occurred more at the edge than on the plane via edge diffusion, even though pulse

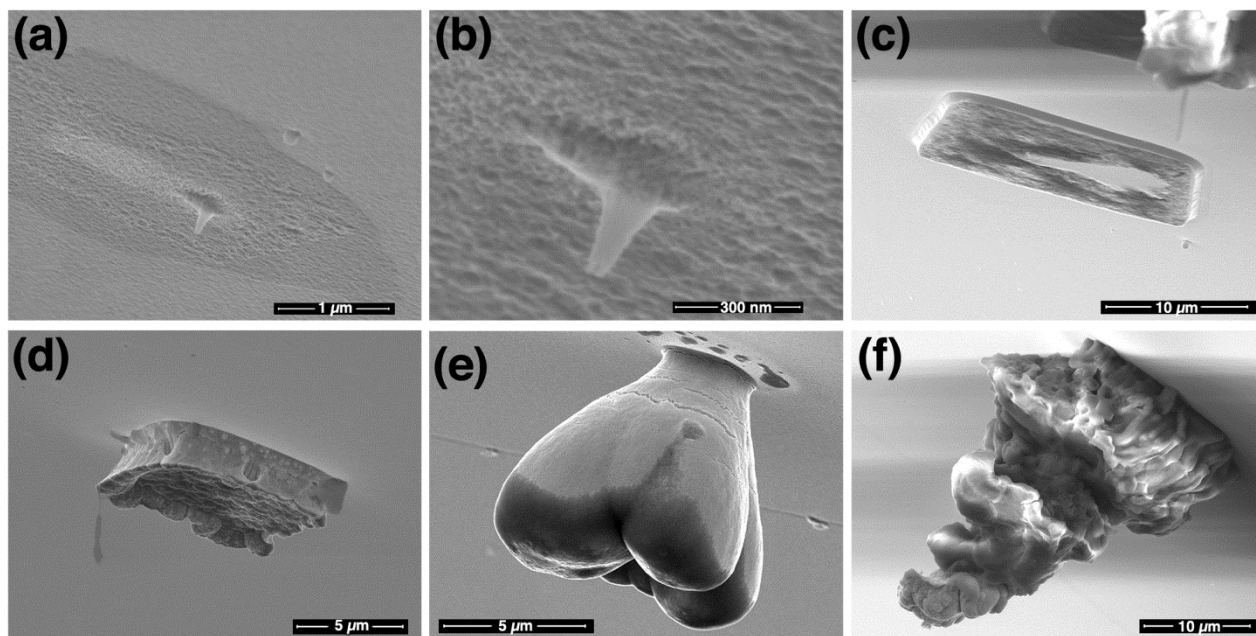


Figure 4. SEM images of various Pt structures produced by different approaches using the HYPER. In (a)-(d), Pt was formed by the contact of the HYPER followed by pulsed deposition: (a) an electrodeposited tack-like Pt structure; (b) a zoomed-in image of the pin area of (a); (c) a plate-like structure with a larger contact area; (d) a thick plate deposited by longer pulsed deposition; (e) the Pt structure obtained by pulling the tip at a regular speed at a constant potential; and (f) an arbitrary structure similar to soft ice cream, fabricated by repeating the pulsed deposition and pulling the tip.

deposition diminishes non-linear diffusion. When a constant potential was applied and the tip was pulled at a regular speed during deposition, the vertex and edge effects were maximized, as shown in Figure 4E, in which the Pt structure grew through four vertices of the electroactive square. Moreover, arbitrary 3D structures were printed by the HYPER by sequential electrodeposition. Figure 4F shows a Pt structure similar to soft ice cream produced by repeated pulsed electrodeposition and pulling of the tip. Notably, the height of the deposited structures was as high as *ca.* 30 μm, demonstrating the ability of the HYPER to deposit materials with a high aspect ratio. HYPER also has the ability to produce metallic structure array based on lateral scan. (See supplementary information) Electrodeposition by the HYPER can be summarized as follows: (1) To date, the minimum feature size obtained by the HYPER was *ca.* 180 nm in diameter, even though the thin and round metallic film was appended due to the inevitable presence of an electrolyte meniscus. When the surface area of the electroactive square was much larger than that of the meniscus, the additional structure disappears. (2) Materials with a high aspect ratio can be fabricated successfully. (3) The HYPER, in conjunction with electrodeposition, potentially enables the deposition of any arbitrary metallic structure if all parameters, such as the potential program for pulse electrodeposition, control of diffusion, tip pulling speed and size of the meniscus, are optimized. We believe that further investigation of our HYPER will provide a new path to affordable 3D nanoprinting.

Conclusions

This work represents the first report of a hydrogel pen being utilized to investigate electrochemical processes in the nanometer-scale regime and to produce 3D metallic structures. The HYPER provides significant advantages in terms of simplicity, size of electrode, reproducibility and cost compared with previous approaches. The theory related to the HYPER

indicates electrochemical behavior similar to that of a typical ultramicroelectrode. We have shown that 3D printing by electrodeposition can be performed using the HYPER. Localized electrochemistry by the HYPER might offer new opportunities in electrochemistry, nanoscience, 3D printing and SPM.

Experimental

Materials

Hard agarose, ferrocenemethanol (97%), Potassium tetrachloroplatinate(II) ($K_2PtCl_4 \geq 99.9\%$), Potassium perchlorate ($KClO_4 \geq 99\%$) and Potassium chloride (99.9%) were purchased from Sigma-Aldrich. Au microdisk electrode (5 μm radius), polishing diamond and polishing alumina were purchased from Bas inc. Polishing micro-cloth pad was purchased from Beuhler. Milli-Q water (18.2 MΩ) was used for all aqueous solutions.

Preparation of hydrogel pen for electrochemical reaction

Agarose solution (8.3 wt% agarose in water) was prepared in a long cylinder-shaped bottle which has a sealing cap. The solution in the bottle was preconditioned in 90°C water bath for an hour. Air bubbles were removed by boiling in microwave (700W) for 30s and Si template was immersed to the bottom of viscous and transparent agarose solution. The bottle which contains solution and template was placed in the 90°C bath again with cap closed and residual air bubbles were removed slowly for additional an hour. After bubbles were completely removed, the solution was cooled down to room temperature slowly with cap closed in water bath (power off) overnight. Agarose gel was detached from the master cautiously and the agarose surface was washed by distilled water. The agarose

body was divided into edged cylinders which have a pyramidal tip on each block by manual cutting. (Hydrogel pen : a pyramidal tip on each agarose cylinder). The hydrogel pens were soaked in aqueous solution which contains 1.7mM ferrocenemethanol and 115mM KClO₄ for electrochemical reaction. The volume of solution for soaking a hydrogel pen was 30 times of the volume of each hydrogel pen to minimize dilution of redox molecules. The hydrogels were soaked for 8hours for complete equilibrium before electrochemical measurement. (Chemical equilibrium of the concentration of hydrogel and solution is in Supplementary Information.)

Instrumentation

Electrochemical measurements were carried out using a CHI 900b potentiostat and Scanning Electrochemical Microscope system (CHI instruments). The electrochemical cell and piezo system were placed in a home-made faradaic cage (Cu, 1mm square mesh) on optical table. Ag/AgCl reference electrode and Pt (wire, 0.5mm diameter) counter electrode were used. Au substrate (100nm thickness Au on Si wafer) was used as working electrode. The working electrode was fixed on piezo motor and its position was controlled by manual stage control mode.

Electrochemical measurement using hydrogel pen

Working electrode (Au substrate) was fixed on piezo motor and insulating glass was placed between the electrode and the motor. The hydrogel pen was placed in electrochemical cell, in which reference and counter electrode were connected and the pyramidal tip of hydrogel was faced to Au electrode surface. Au substrate was approached from the above of hydrogel tip to the close proximity of the tip. USB microscope is used for brief monitoring of the approach of the electrode and accurate contact event was confirmed from the electrochemical signal generated from the circuit closing by the contact of hydrogel (electrolyte) and Au substrate (working electrode). The potential for oxidation of ferrocenemethanol (0.5V) was being applied on the working electrode for entire measurement. In the close proximity, Au substrate was approached by a small distance (100nm~1µm) at once in monitoring of current. The sharp charging current signal was generated in the moment of contact and stable steady-state current was shown in a few seconds. After confirmation of contact, electroactive area could be controlled by additional approach and current feedback.

3-dimensional electrodeposition of Platinum using hydrogel pen

20mM K₂PtCl₄, 115mM KClO₄ aqueous solution was used as soaking solution and aforementioned electrochemical setup and approach method was employed. Working electrode was approached by 100nm to minimize contact area and the potential (0.6V), in which Pt reduction doesn't occur and only the charging current could be generated, was applied. The sharp charging current (Figure S9) is generated by the contact and the reduction of Pt does not occur in this potential. After the confirmation of contact, potential for reduction of Pt, pulse repetition (-0.4V for 0.01s, 0.3V for 0.03s), was applied and z-position of working electrode was controlled by piezo controller.

Acknowledgements

J.K. acknowledges the support from the National Research Foundation of Korea (NRF) grant funded by the Korea government (MSIP) (No.20090083525). S.H. acknowledges the support from Basic Science Research Program through the National Research Foundation of Korea (NRF) funded by the Ministry of Education, Science, and Technology (2012R1A1A2006038).

Notes and references

^a Department of Chemistry, Korea Advanced Institute of Science and Technology (KAIST), Daejeon 305-701, Republic of Korea

E-mail : juhyoun_kwak@kaist.ac.kr

^b Department of Advanced Material Chemistry, Korea University, Sejong 339-700, Republic of Korea

E-mail : sphwang@korea.ac.kr

§ Equal contribution.

† Electronic Supplementary Information (ESI) available: [Fabrication of silicon master, experimental determination of the mass transport coefficient within hydrogel and numerical simulation about mass transport behavior within HYPER.]. See DOI: 10.1039/b000000x/

1. B. Y. Ahn, E. B. Duoss, M. J. Motala, X. Y. Guo, S. I. Park, Y. J. Xiong, J. Yoon, R. G. Nuzzo, J. A. Rogers and J. A. Lewis, *Science*, 2009, **323**, 1590-1593.
2. J. Hruby, *Mrs Bull.*, 2001, **26**, 337-340.
3. M. Campbell, D. N. Sharp, M. T. Harrison, R. G. Denning and A. J. Turberfield, *Nature*, 2000, **404**, 53-56.
4. S. Jeon, J. U. Park, R. Cirelli, S. Yang, C. E. Heitzman, P. V. Braun, P. J. A. Kenis and J. A. Rogers, *Proc. Natl. Acad. Sci. USA*, 2004, **101**, 12428-12433.
5. S. Kawata, H. B. Sun, T. Tanaka and K. Takada, *Nature*, 2001, **412**, 697-698.
6. B. D. Gates, Q. B. Xu, M. Stewart, D. Ryan, C. G. Willson and G. M. Whitesides, *Chem. Rev.*, 2005, **105**, 1171-1196.
7. K. Sieradzki, S. R. Brankovic and N. Dimitrov, *Science*, 1999, **284**, 138-141.
8. S. J. Hurst, E. K. Payne, L. D. Qin and C. A. Mirkin, *Angew. Chem. Int. Edit.*, 2006, **45**, 2672-2692.
9. M. P. Zach, K. H. Ng and R. M. Penner, *Science*, 2000, **290**, 2120-2123.
10. E. J. Menke, M. A. Thompson, C. Xiang, L. C. Yang and R. M. Penner, *Nat. Mater.*, 2006, **5**, 914-919.
11. R. Schuster, V. Kirchner, P. Allongue and G. Ertl, *Science*, 2000, **289**, 98-101.
12. C. Kranz, *Analyst*, 2014, **139**, 336-352.
13. C. G. Williams, M. A. Edwards, A. L. Colley, J. V. Macpherson and P. R. Unwin, *Anal. Chem.*, 2009, **81**, 2486-2495.
14. M. E. Snowden, A. G. Güell, S. C. S. Lai, K. McKelvey, N. Ebejer, M. A. O'Connell, A. W. Colburn and P. R. Unwin, *Anal. Chem.*, 2012, **84**, 2483-2491.
15. J. C. Byers, A. G. Güell and P. R. Unwin, *J. Am. Chem. Soc.*, 2014, **136**, 11252-11255.
16. Y. Yatziv, I. Turyan and D. Mandler, *J. Am. Chem. Soc.*, 2002, **124**, 5618-5619.
17. C. Laslau, D. E. Williams, B. Kannan and J. Trivas-Sejdic, *Adv. Func. Mater.*, 2011, **21**, 4607-4616.
18. A. J. Bard, F. R. F. Fan, J. Kwak and O. Lev, *Anal. Chem.*, 1989, **61**, 132-138.
19. S. Lai, R. A. Lazenby, P. M. Kirkman and P. R. Unwin, *Chemical Science*, 2014. DOI: 10.1039/C4SC02792B
20. G. Zhang, P. M. Kirkman, A. N. Patel, A. S. Cuharuc, K. McKelvey and P. R. Unwin, *J. Am. Chem. Soc.*, 2014, **136**, 11444-11451.
21. D. Momotenko, F. Cortes-Salazar, A. Lesch, G. Wittstock and H. H. Girault, *Anal. Chem.*, 2011, **83**, 5275-5282.

22. F. Cortés-Salazar, A. Lesch, D. Momotenko, J.-M. Busnel, G. Wittstock and H. H. Girault, *Anal. Methods*, 2010, **2**, 817.
23. F. Cortés-Salazar, D. Momotenko, H. H. Girault, A. Lesch and G. Wittstock, *Anal. Chem.*, 2011, **83**, 1493-1499.
24. Y. Takahashi, A. I. Shevchuk, P. Novak, Y. J. Zhang, N. Ebejer, J. V. Macpherson, P. R. Unwin, A. J. Pollard, D. Roy, C. A. Clifford, H. Shiku, T. Matsue, D. Klenerman and Y. E. Korchev, *Angew. Chem. Int. Edit.*, 2011, **50**, 9638-9642.
25. P. Novak, C. Li, A. I. Shevchuk, R. Stepanyan, M. Caldwell, S. Hughes, T. G. Smart, J. Gorelik, V. P. Ostanin, M. J. Lab, G. W. J. Moss, G. I. Frolenkov, D. Klenerman and Y. E. Korchev, *Nat. Methods*, 2009, **6**, 935-935.
26. P. S. Dobson, J. M. R. Weaver, M. N. Holder, P. R. Unwin and J. V. Macpherson, *Anal. Chem.*, 2005, **77**, 424-434.
27. C. Keplinger, J. Y. Sun, C. C. Foo, P. Rothmund, G. M. Whitesides and Z. G. Suo, *Science*, 2013, **341**, 984-987.
28. R. Klajn, M. Fialkowski, I. T. Bensemann, A. Bitner, C. J. Campbell, K. Bishop, S. Smoukov and B. A. Grzybowski, *Nat. Mater.*, 2004, **3**, 729-735.
29. F. W. Huo, Z. J. Zheng, G. F. Zheng, L. R. Giam, H. Zhang and C. A. Mirkin, *Science*, 2008, **321**, 1658-1660.
30. Y. Jung and J. Kwak, *B. Kor. Chem. Soc.*, 1994, **15**, 209-213.
31. J. Labille, N. Fatin-Rouge and J. Buffle, *Langmuir*, 2006, **23**, 2083-2090.
32. N. Fatin-Rouge, A. Milon, J. Buffle, R. R. Goulet and A. Tessier, *J. Phys. Chem. B*, 2003, **107**, 12126-12137.
33. I. J. Cutress, E. J. F. Dickinson and R. G. Compton, *J. Electroanal. Chem.*, 2010, **638**, 76-83.
34. I. J. Cutress and R. G. Compton, *J. Electroanal. Chem.*, 2010, **645**, 159-166.
35. Z. Porat, J. C. Crooker, Y. N. Zhang, Y. LeMest and R. W. Murray, *Anal. Chem.*, 1997, **69**, 5073-5081.
36. W. Shim, A. B. Braunschweig, X. Liao, J. N. Chai, J. K. Lim, G. F. Zheng and C. A. Mirkin, *Nature*, 2011, **469**, 516-521.
37. R. D. Piner, J. Zhu, F. Xu, S. H. Hong and C. A. Mirkin, *Science*, 1999, **283**, 661-663.
38. Y. H. Liu, D. Gokcen, U. Bertocci and T. P. Moffat, *Science*, 2012, **338**, 1327-1330.
39. M. S. Chandrasekar and M. Pushpavanam, *Electrochim. Acta.*, 2008, **53**, 3313-3322.